British Journal of Pharmacology

DOI:10.1111/bph.12427
www.brjpharmacol.org

RESEARCH PAPER

In vitro and *in vivo* anti-tumour effects of MPT0B014, a novel derivative aroylquinoline, and in combination with erlotinib in human non-small-cell lung cancer cells

An-Chi Tsai[1], Hui-Chen Pai[2], Chih-Ya Wang[2], Jing-Ping Liou[1], Che-Ming Teng[2], Jing-Chi Wang[3] and Shiow-Lin Pan[3]

[1]*School of Pharmacy, College of Pharmacy, Taipei Medical University, Taipei, Taiwan,* [2]*Pharmacological Institute, College of Medicine, National Taiwan University, Taipei, Taiwan, and* [3]*The PhD Program for Cancer Biology and Drug Discovery, College of Medical Science and Technology, Taipei Medical University, Taipei, Taiwan*

Correspondence
Shiow-Lin Pan, The PhD Program for Cancer Biology and Drug Discovery, College of Medical Science and Technology, Taipei Medical University, No. 250, Wu-Hsing St., Taipei 11031, Taiwan. E-mail: slpan@tmu.edu.tw

Classification: Antibiotics and Chemotherapeutics.

An-Chi Tsai, Hui-Chen Pai and Chih-Ya Wang contributed equally to this work.

Keywords
mitosis arrest; apoptosis; Mcl-1; P-gp; NSCLC; MPT0B014

Received
15 May 2013
Revised
30 August 2013
Accepted
11 September 2013

BACKGROUND AND PURPOSE

The purpose of the current study was to assess a novel anti-cancer drug, MPT0B014, which is not a substrate for the P-glycoprotein (P-gp) transporter, alone and in combination with erlotinib, against human non-small cell lung cancer (NSCLC).

EXPERIMENTAL APPROACH

Cytotoxicity in human NSCLC cell lines was assessed by sulforhodamine B and 3-(4,5-dimethylthiazol-2-yl)-2,5-diphenyltetrazolium bromide assays. Cell cycle phase distributions were estimated with FACScan flow cytometry. Protein expression was detected by Western blotting analysis. Efflux of rhodamine 123 or calcein-acetoxymethylester was used to study the P-gp profile. The A549 xenograft model in mice was used to assess *in vivo* anti-tumour activity.

KEY RESULTS

MPT0B014 showed potent anti-proliferative activity against A549, H1299 and H226 cells. It induced G2/M arrest with down-regulation of *Cdc* (*Tyr15*) and *Cdc25C*, and up-regulation of *cyclin B1*, phospho-*Cdc2* (*Thr161*) and *Aurora A/B*. P-gp-overexpressing National Cancer Institute/Adriamycin-Resistant cells were also sensitive to B014. B014-induced loss of Mcl-1 was accompanied by activation of caspases-3, -7, -8 and -9, and initiation of apoptosis. B014 in combination with erlotinib caused significant tumour inhibition *in vitro* and *in vivo*.

CONCLUSIONS AND IMPLICATIONS

MPT0B014 exerted cytotoxicity against human NSCLC cell lines with little susceptibility to P-gp. Combined with the EGF receptor inhibitor, erlotinib, MPT0B014 exerted significant growth inhibition of A549 cells both *in vitro* and *in vivo*. B014 could be useful as an anti-cancer agent.

Abbreviations
NSCLC, non-small cell lung cancer; P-gp, p-glycoprotein; TGD, tumour growth delay; TKI, TK inhibitor

Introduction

Lung cancer is the most common cancer and is a major cause of cancer-related mortality in the United States and worldwide. The American Cancer Society estimated that there would be 226 160 new cases and approximately 160 340 deaths from this disease in the United States in 2012. Non-small cell lung cancer (NSCLC), mainly adenocarcinoma, squamous cell carcinoma and large-cell carcinoma, comprise approximately 85% of these cases (Breathnach *et al.*, 2001; Reungwetwattana *et al.*, 2012). Most patients with NSCLC are diagnosed with locally advanced or metastatic disease and are associated with a 5 year survival rate of 17% (Akin *et al.*, 2012; Siegel *et al.*, 2012). Despite treatments with traditional chemotherapeutic agents such as paclitaxel, carboplatin, etoposide, vincristine, cyclophosphamide, cisplatin and EGF receptor (EGFR) kinase inhibitors, relapse occurs in most cases and overall survival is poor, particularly with late-stage NSCLC (Francis and Solomon, 2010; Sangodkar *et al.*, 2010; Bareschino *et al.*, 2011). Thus, there is an urgent need for more effective therapeutic agents that improve pharmacological profiles and increase survival.

Microtubules, which are dynamic structures consisting of α- and β-tubulin heterodimers, are a major component of the cellular cytoskeleton and are essential for cell division, intracellular material transportation, organelle localization and cell motility (Nogales, 2001; Risinger *et al.*, 2009). Compounds that target microtubules have potential clinical utility and are generally classified into two main groups. One group, which includes taxanes, promotes microtubule polymerization, whereas the other, which includes the vinca alkaloids and colchicines, inhibits microtubule polymerization (Jordan and Wilson, 2004). These microtubule-targeting agents primarily alter the normal dynamic equilibrium, resulting in stabilization or destabilization of microtubules, causing a mitotic slowing or blockade at the metaphase/anaphase transition and the consequent triggering of apoptosis (Bhalla, 2003; Honore *et al.*, 2005). They are clinically effective against various human cancers such as breast cancer, ovarian cancer and NSCLC. Although these agents are widely used clinically, there are numerous drawbacks. Multidrug resistance is the major clinical obstacle in cancer therapy (Perez, 2009; Kavallaris, 2010). Overexpression of the ATP-driven membrane drug efflux pump P-glycoprotein (P-gp) is the best-characterized mechanism of drug resistance to microtubule inhibitors (Bhat and Setaluri, 2007). Thus, identification of natural or synthetic compounds with therapeutic effects against tumours, particularly multidrug resistant tumours, remains an attractive goal.

Apoptosis comprises a series of typical morphological and biochemical events, including cell shrinkage, nuclear fragmentation, chromatin condensation and rapid phagocytosis by neighbouring cells (Taylor *et al.*, 2008). Caspase cascades have been shown to play central roles in the execution of apoptosis. Activation of caspases results in the cleavage and activation of numerous cellular substrates, including PARP, a DNA repair enzyme that is activated by DNA strand breaks and catalyses poly(ADP-ribosyl)ation of various nuclear proteins. In addition, distinct caspase-activating cascades have been characterized. In extrinsic apoptotic pathways, the initiator caspase-8 is activated by death receptors, and in intrinsic pathways, the initiator caspase-9 is induced by cytotoxic agents (Munoz-Pinedo, 2012).

In this study, we tested the effects of MPT0B014 (hereafter B014), an aroylquinoline derivative, on tubulin interaction and examined its anti-tumour activities in NSCLC cell lines, as well as its ability to overcome drug resistance. We also explored possible molecular mechanisms by which B014 might affect cell cycle progression and apoptosis. Further, we investigated whether B014 was effective in killing A549 cells alone or in combination with erlotinib *in vitro* and *in vivo*. Our data suggest that B014 is a promising therapeutic candidate for treating patients with NSCLC.

Methods

Cell culture

Human NSCLC cell lines (p53 wild-type A549, p53 null H1299, p53 mutant H226 and *L858R/T790M*-EGFR H1975) were purchased from American Type Culture Collection (Manassas, VA, USA). The P-gp-overexpressing human ovarian carcinoma cells National Cancer Institute/Adriamycin-Resistant (NCI/ADR-RES) was obtained from the National Cancer Institute (Frederick, MD, USA). HUVECs were purchased from the Bioresource Collection and Research Center (BCRC, Hsinchu, Taiwan). All NSCLC cell lines and NCI/ADR-RES cells were cultured in RPMI 1640 medium with 10% (v/v) FBS. HUVECs were maintained in M199 medium supplemented with 20% (v/v) heat-inactivated FBS, ECGs and penicillin (100 $U \cdot mL^{-1}$)/streptomycin (100 $\mu g \cdot mL^{-1}$)/amphotericin (0.25 $\mu g \cdot mL^{-1}$) at 37°C in a humidified incubator containing 5% CO_2/95% air.

Cell proliferation assay

Cell proliferation was determined using the sulforhodamine B (SRB) assay. Growing cells were seeded into 96-well plates at a density of 5×10^3 cells per well and allowed to adhere overnight. Cells were fixed with 10% trichloroacetic acid (TCA) to characterize cell populations at the time of test drug addition (T_0). After additional incubation with or without test compounds in medium containing 5% FBS for 48 h, the cells were fixed with 10% TCA and stained with 0.4% SRB (w/v) in 1% acetic acid (v/v). The unbound dye was removed by washing with 1% acetic acid, and the protein-bound dye was subsequently extracted using 10 mM Tris-base to determine

the absorbance at 515 nm. Using the absorbance measurements taken at time zero (T_0), in control conditions (C), and after incubation with test drugs (T), the percentage growth was calculated as $100 - [(T - T_0)/(C - T_0)] \times 100$. IC_{50} was calculated as the test drug concentration that reduced cell proliferation by 50%.

Cell viability assay

Cell viability was evaluated using the MTT assay. Growing cells were seeded in 96-well plates and treated on the following day with or without various concentrations of test compounds for 48 h. MTT solution (0.5 mg·mL^{-1} in RPMI 1640) was added to all wells, the plates were incubated for additional 1 h at 37°C and then formazan crystals were dissolved in DMSO. The plates were read using an automated microplate spectrophotometer at 550 nm. IC_{50} was calculated as the test drug concentration that caused 50% growth inhibition.

Cell cycle analysis

Cell cycle progression was determined using flow cytometry. A549, H1299 and H226 cells were plated onto 6-well plates at a final density of 250 000 cells per well, treated with test compounds, and then trypsinized, collected and fixed in ice-cold 75% ethanol overnight at –20°C. After centrifugation, the fixed cells were rinsed with ice-cold PBS and incubated with 0.1 M phosphate/citric acid buffer (0.2 M Na_2HPO_4, 0.1 M citric acid, pH 7.8) at room temperature for 30 min. The cells were then centrifuged and resuspended in PI staining buffer containing RNase (100 μg·mL^{-1}), PI (80 μg·mL^{-1}) and 0.1% Triton X-100 (v/v; Sigma-Aldrich, St Louis, MO, USA) in darkness. The DNA content was analysed using a FACScan flow cytometer with CellQuest software (Becton Dickinson, San Jose, CA, USA).

In vitro *tubulin polymerization assay*

Microtubule assembly was assessed using the CytoDYNAMIX Screen kit (BK006P; Cytoskeleton Inc., Denver, CO, USA). Purified porcine tubulin proteins (>99% purity) were suspended in G-PEM buffer containing 80 mM PIPES, 2 mM $MgCl_2$, 0.5 mM EGTA, 1 mM GTP (pH 6.9) and 15% glycerol in the absence or presence of indicated compounds at 4°C. The mixture was immediately transferred to pre-warmed 96-well plates, and absorbance was measured at 340 nm every 1 min for 30 min using a 37°C plate reader (SpectraMAX Plus; Molecular Devices Inc., Sunnyvale, CA, USA).

Immunofluorescence confocal microscopy

A549 cells were sparsely seeded in 8-well chamber slides and allowed to adhere overnight before treating with or without indicated compounds. At the specified time point, cells were fixed in cold methanol at –20°C for 15 min, washed with PBS and blocked with 1% PBS plus 0.1% Triton X-100 for 30 min at 37°C. After incubation with a monoclonal anti-β-tubulin antibody, diluted 1:500 in PBS, for 1 h at 37°C, cells were washed in PBS and incubated with FITC-conjugated anti-mouse IgG diluted 1:50 in PBS, for 45 min at 37°C. Finally, DAPI staining was performed and slides were imaged using a Leica TCS SP2 confocal spectral microscope (Buffalo, NY, USA).

Apoptosis assay

Compound-induced apoptosis was assessed using a Cell Death Detection ELISA^{PLUS} kit (Roche Diagnostics, Basel, Switzerland) according to the manufacturer's instructions. Briefly, apoptotic oligonucleosomal fragmentation of DNA was directly detected after 48 h of treatment. Spectrophotometric data were acquired using the ELISA reader at a wavelength of 405 nm, with a reference wavelength of 490 nm.

Nuclear protein extraction

Following treatment with B014, cells were trypsinized, collected, scraped with buffer A (1.5 mM $MgCl_2$, 10 mM KCl, 0.5 mM DTT, 1% Nonidet P-40 and protease inhibitors, pH 7.9) and incubated on ice for 15 min. After centrifugation at 400 × *g* for 5 min at 4°C, the supernatant (the cytoplasmic protein fraction) was removed and the pellets was suspended in buffer C (20 mM HEPES, 420 mM NaCl, 1.5 mM $MgCl_2$, 0.2 mM EDTA, 0.5 mM DTT, 0.2 mM PMSF and 25% glycerol, pH 7.9) on ice for 30 min. The suspension was then centrifuged at 11 000 × *g* for 10 min at 4°C, and the final supernatant (the nuclear extract fraction) was frozen at –20°C.

Transient transfection and Western blot analysis

A549 cells were transiently transfected with human Mcl-1 (25375) plasmid (Addgene, Cambridge, MA, USA) and Mcl-1 small-interfering RNA (5′ GGACUUUUAGAUUUAGUGA dTdT 3′) (Applied Biosystems/Ambion, Austin, TX, USA) using Lipofectamine 2000 according to the manufacturer's protocol. Eight hours after transfection, the cells were treated with indicated compounds for 48 h. For Western blot analysis, cells were harvested using a lysis buffer (2.5 mM sodium pyrophosphate, 1 mM EGTA, 1 mM EDTA, 150 mM NaCl, 1 mM PMSF, 1 mM Na_3VO_4, 1 mM NaF, 0.1% Triton X-100 in 20 mM Tris–HCl buffer, pH 7.5), and then centrifuged at 11 000 × *g* for 30 min. Cell lysates were collected and analysed by immunoblotting with specific antibodies. The signals were visualized using an enhanced chemiluminescence detection system (Amersham, Buckinghamshire, UK).

P-gp activity assay

Rhodamine-123 (Rh-123) or calcein-acetoxymethylester (calcein-AM) was used in efflux assays to assess the transport activity of P-gp. For the Rh-123 assay, NCI/ADR-RES cells were pretreated with or without indicated agents for 60 min and then incubated with Rh-123 in the dark for a further 60 min at 37°C. After incubation, the cells were washed with ice-cold PBS to remove excess Rh-123 and collected after trypsinization. Bound agents were analysed using a FACScan flow cytometer. For the calcein-AM assay, NCI/ADR-RES cells were seeded in 96-well culture plates at a density of 5×10^4 cells per well in 100 μL of culture medium and allowed to adhere overnight. After incubation for 30 min with vehicle control or experimental compounds, calcein-AM/Hoechst dye staining solution was added to each well and incubated for a further 30 min. At the end of the treatment, cells that took up calcein-AM were detected using fluorescence filters (excitation, 485 nm; emission, 535 nm).

A549 xenograft models

All animal care and experimental studies were conducted in accordance with the guidelines of the Animal Care and Use Committee at National Taiwan University. All studies involving animals are reported in accordance with the ARRIVE guidelines for reporting experiments involving animals (Kilkenny *et al.*, 2010; McGrath *et al.*, 2010). A total of 29 mice were used in the experiments described here. Nude athymic mice (male, 5–6 weeks) were s.c. injected in the back with 2×10^6 A549 cells per mouse. When tumour volumes reached approximately 100 mm^3, mice were randomized by tumour sized into four treatment groups as follows: C/T vehicle (0.5% carboxymethyl cellulose/0.1% Tween-80 in double distilled H_2O; Wako, Osaka, Japan), 100 $mg \cdot kg^{-1}$ B014, 25 $mg \cdot kg^{-1}$ erlotinib and B014 plus erlotinib in C/T vehicle every day. Mice received i.v./i.p. doses of B014 and p.o. gavage doses of erlotinib. Tumour volumes were calculated using calliper measurements twice per week using the formula volume (mm^3) = (length × $width^2$)/2. Body wts were measured daily during the first week and twice per week thereafter. Tumours in all groups were allowed to reach an end point volume of 1200 mm^3. Statistical and graphical analyses were performed as described previously (Huang *et al.*, 2012).

Statistical analysis

Data are expressed as means ± SEM for the indicated number of separate experiments. Statistical difference was assessed using Student's *t*-test, and *P*-values < 0.05 were considered significant.

Materials

B014 was synthesized by Professor Jing-Ping Liou's Research Laboratories (School of Pharmacy, College of Pharmacy, Taipei Medical University, Taipei, Taiwan). RPMI 1640, FBS and trypsin–EDTA were purchased from Gibco BRL Life Technologies (Grand Island, NY, USA). Sulforhodamine B (SRB), 3-(4,5-dimethylthiazol-2-yl)-2,5-diphenyltetrazolium bromide (MTT), propidium iodide (PI) and FITC-conjugated anti-mouse IgG were obtained from Sigma (St. Louis, MO, USA). DAPI was purchased from Roche Molecular Biochemicals (Mannheim, Germany). The following antibodies were used: cdc2 (Thr161), cdc2 (Tyr15), Aurora A, Aurora B, BID, caspase-8 and caspase-9 (Cell Signaling Technology, Beverly, MA, USA); cyclin B1, cdc25C, cdc2, Bcl-2, p-Bcl-2, Bcl-xL, BAX, Mcl-1, Bak and PARP (Santa Cruz Biotechnology, Santa Cruz, CA, USA); MPM2 (Ser^{161}/Thr^{97}) (Upstate Biotechnology, Temecula, CA, USA); caspase-3 (Imgenex, San Diego, CA, USA); and caspase-7 (BD Biosciences, San Joes, CA, USA).

Results

Effects of B014 on cell proliferation and survival in vitro

Initially, we evaluated the *in vitro* anti-proliferative activities of B014 (Figure 1A) in the three human NSCLC cell lines A549, H1299 and H226 using the SRB assay. B014 inhibited cell growth in a concentration-dependent manner, with IC_{50} values as shown in Figure 1B. The MTT assay was also performed to evaluate the effect of B014 on cell viability. As shown in Figure 1C, B014 showed potent cytotoxicity against A549, H1299 and H226, but showed much less activity against HUVECs (Figure 1D). These data indicate that human NSCLC cells were much more sensitive to cell cytotoxicity induced by B014, in comparison with normal cells.

Effects of B014 on cell cycle progression and G2/M regulatory proteins

To investigate the mechanisms responsible for the anti-proliferative effects of B014, we examined the cell cycle distribution profiles of B014-treated human NSCLC cell lines (A549, H1299 and H226) using flow cytometry with PI DNA labelling. B014 treatment for 24 h led to notable accumulation of cells in the G2/M phase. At 48 h, sub-G1 apoptotic cell populations were increased in a concentration-dependent manner (Figure 2A). The bar graphs (Figure 2B) provide an overview of the percent cell population in various cell cycle profiles upon B014 treatment over time. Specifically, cells in the G2/M phase began to rise at 12 h post-treatment and peaked at 24 h. Following this, there was an emergence of cells in the sub-G1 population phase until 48 h.

Effect of B014 on G2/M regulatory proteins

Next, we examined the effect of B014 on the regulatory proteins involved in G2/M arrest signalling pathways using immunoblotting assays. As shown in Figure 2C, treatment of NSCLC cell lines with B014 resulted in a marked increase in expression of the mitosis marker MPM2 and the proteins cyclin B1, Cdc2, Thr161, Aurora A and Aurora B in a concentration-dependent manner. B014 treatment decreased the expression of Cdc (Tyr15) and Cdc25C, whereas total protein levels of Cdc2 did not change. The same effects were observed in a time-dependent manner in B014-treated A549 cells (Figure 2D). Furthermore, B014 notably enhanced cyclin B1 protein levels in the nuclear fraction in A549 cells, indicating arrest in M phase (Figure 2E).

Effects of B014 on microtubule organization

Because B014 caused a significant mitotic arrest, we investigated its effects on microtubule organization using a cell-free tubulin polymerization assay. As shown in Figure 3A, B014 significantly inhibited tubulin polymerization, similar to the microtubule-destabilizing agent vincristine. Further, immunofluorescence analysis was used to evaluate the effect of test compounds on microtubule network arrangement and distribution. B014-treated A549 cells exhibited disruption of the microtubule cytoskeleton, similar to that in vincristine-treated cells (Figure 3B).

Effect of B014 on apoptosis

Induction of apoptosis by B014 was indicated by the appearance of a sub-G1 population in NSCLC cells, as confirmed by enzyme immunoassays for histone-associated DNA fragments. DNA fragmentation increased with B014 treatment in a concentration-dependent manner (Figure 4A). Further evidence of B014-induced apoptosis was provided by experiments showing B014-induced activation of caspases-3, -7, -8 and -9, and cleavage of PARP in a time- and concentration-dependent manner (Figure 4B,C).

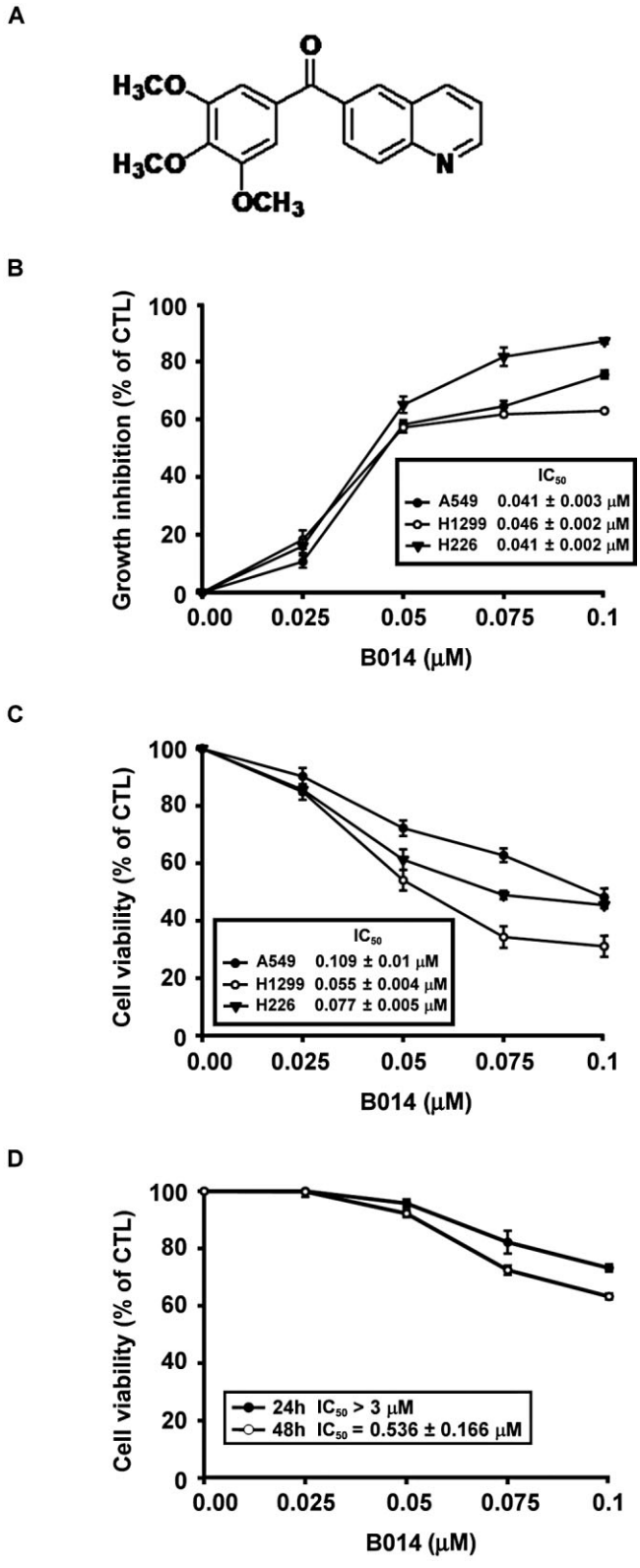

Figure 1

Growth inhibition of NSCLC cell lines by B014. (A) Chemical structure of B014. (B) A549, H1299 and H226 cells were incubated in the absence or presence of the indicated concentrations of B014 for 48 h. Cell growth inhibition was determined using the SRB assay. (C) Cytotoxicity was evaluated using the MTT assay. (D) HUVECs were treated with indicated concentrations of B014 for 24 and 48 h. Cytotoxicity was evaluated using the MTT assay. Data shown are means ± SE of at least three independent experiments.

Effect of B014 on proteins of the Bcl-2 family

Proteins of Bcl-2 family participate in both pro- and anti-apoptotic processes. In A549 cells, B014 did not affect the expression of the anti-apoptotic (Bcl-2, Bcl-xL) or pro-apoptotic (BAX, Bak, BID) proteins (Figure 4D). However, Cdk1/cyclin B induces Bcl-xL/Bcl-2 phosphorylation during mitotic arrest. In this study, we found that B014 significantly induced Bcl-2 phosphorylation (Figure 4D). In addition, B014 down-regulated Mcl-1 expression in a concentration-dependent manner. Moreover, exogenous Mcl-1 overexpression rescued A549 cells from B014-mediated cell growth inhibition (Figure 4E), and knockdown of Mcl-1 by RNA interference did not affect B014-induced apoptosis (Figure 4F), indicating the importance of Mcl-1 in B014-induced apoptosis.

Effect of B014 on P-gp activity

P-gp-mediated multidrug resistance is a major limiting factor in the efficacy of most microtubule-targeting agents. Thus, we examined the susceptibility of B014 to P-gp using the P-gp-overexpressing NCI/ADR-RES cell line. The cytotoxicity of B014 was not markedly different in P-gp-rich cells compared with that in A549 cells, with IC_{50} values of about 30nM (Figure 5A,B). In contrast, the IC_{50} values of paclitaxel and vincristine in this cell line were about 8000 nM (Figure 5C). To confirm these observations, we further used flow cytometry to monitor accumulation of Rh-123 in B014-treated NCI/ADR-RES cells. As shown in Figure 5D, Rh-123 efflux was inhibited by co-treatment with the P-gp inhibitor verapamil or cyclosporine A. However, Rh-123 accumulation was not increased in NCI/ADR-RES cells after incubation with B014. Moreover, in calcein-AM (a substrate for P-gp) efflux experiments, both verapamil and cyclosporine A significantly increased calcein fluorescence, whereas the efflux of calcein-AM was not affected by B014 at concentrations up to 3.0 μM (Figure 5D). These results suggest that B014 does not interfere with the function of P-gp in tumour cells.

Effect of B014 in combination with erlotinib in vitro *and* in vivo

Erlotinib has proven efficacy in advanced NSCLC (Brown and Shepherd, 2005). Thus, we examined the *in vitro* effect of combined treatment with B014 and erlotinib on cell growth inhibition using a combination index (CI) in A549 and H1975 cells. The combined treatment produced CI values less than 1, suggesting synergistic cytotoxicity (Figure 6A). Moreover, significant induction of cell apoptosis was observed using enzyme immunoassays for histone-associated DNA fragments (Figure 6B). Next, we determined *in vivo* anti-tumour activity of this combination using the A549 xenograft model. The combined treatment resulted in more significant tumour growth delay (28%) compared with B014 (7%) or erlotinib (7%) treatments alone (Figure 6C).

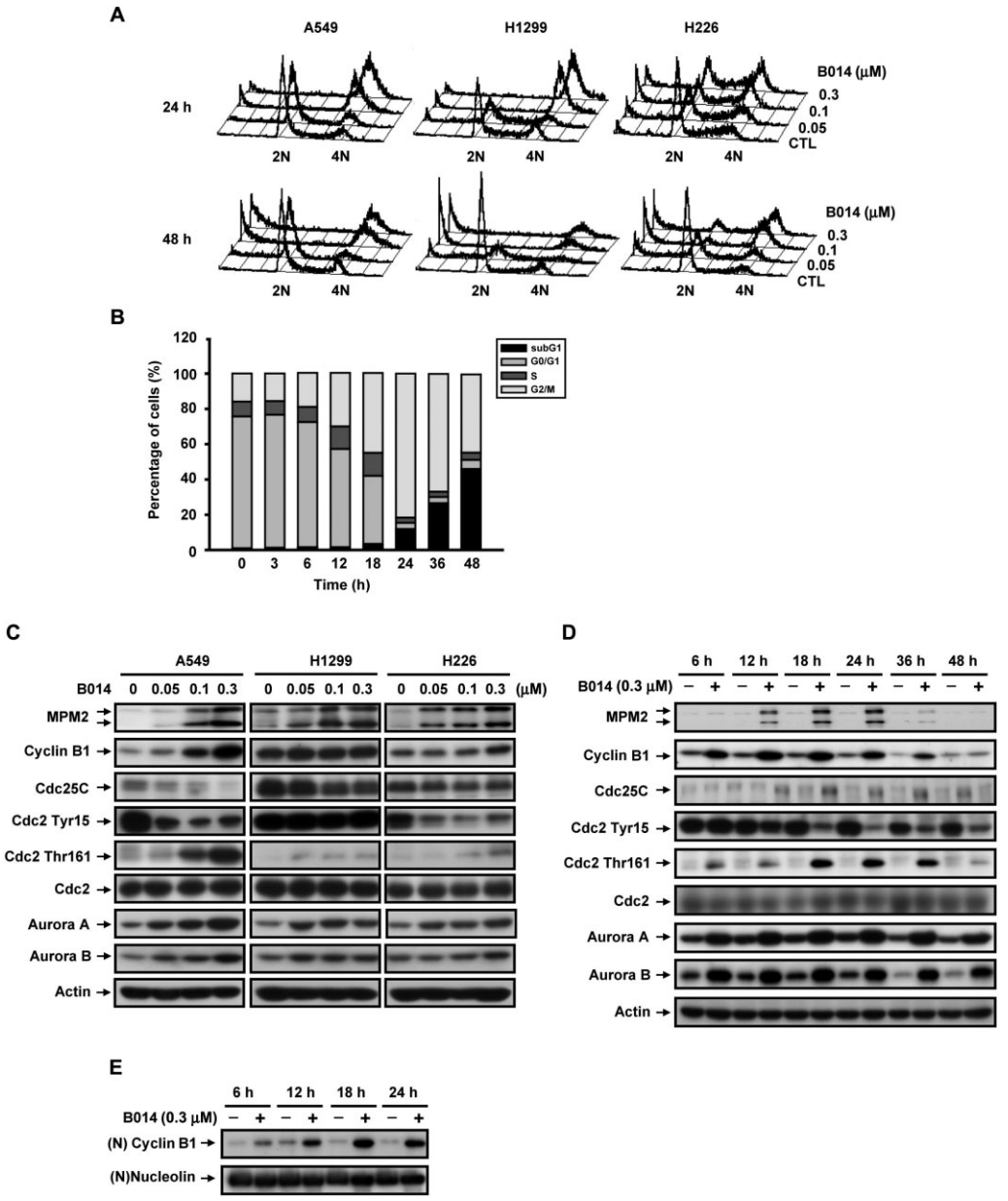

Figure 2

Effect of B014 on cell cycle profiles. (A) A549, H1299 and H226 cells were treated without or with indicated concentrations of B014 for 24 and 48 h, stained with PI, and analysed using FACScan flow cytometry. The X axis shows the total DNA content of cells. The Y axis shows the number of cells. The Z axis indicates the concentration of B014. (B) A549 cells were exposed to 0.3 μM B014 for indicated times and stained with PI. Cell cycle distributions were analysed by FACScan flow cytometry. (C) A549, H1299 and H226 cells were incubated without or with the indicated concentrations of B014 for 24 h, and whole-cell extracts were prepared and analysed using the indicated antibodies. (D) Expression of G2/M regulatory proteins was investigated. After treatment with 0.3 μM B014 for indicated times, cells were harvested, lysed and subjected to Western blot analysis. (E) Nuclear extracts of B014-treated A549 cells were probed with cyclin B1 antibody using Western blot analysis.

According to log-rank analysis, the combination of B014 and erlotinib produced significantly higher anti-tumour activity ($P < 0.0001$). The growth of A549 cancer cell xenografts was suppressed by 11, 21 and 49% (tumour growth inhibition) after treatment with B014, erlotinib and B014 plus erlotinib respectively (Figure 6D, left panel). However, no significant differences in body weight were observed during treatments (Figure 6D, right panel). These data may suggest that the combination of B014 and erlotinib significantly improved tumour inhibition *in vitro* and *in vivo*.

Discussion

Although conventional microtubule-targeting agents such as paclitaxel and vinflunine are available for treatment of

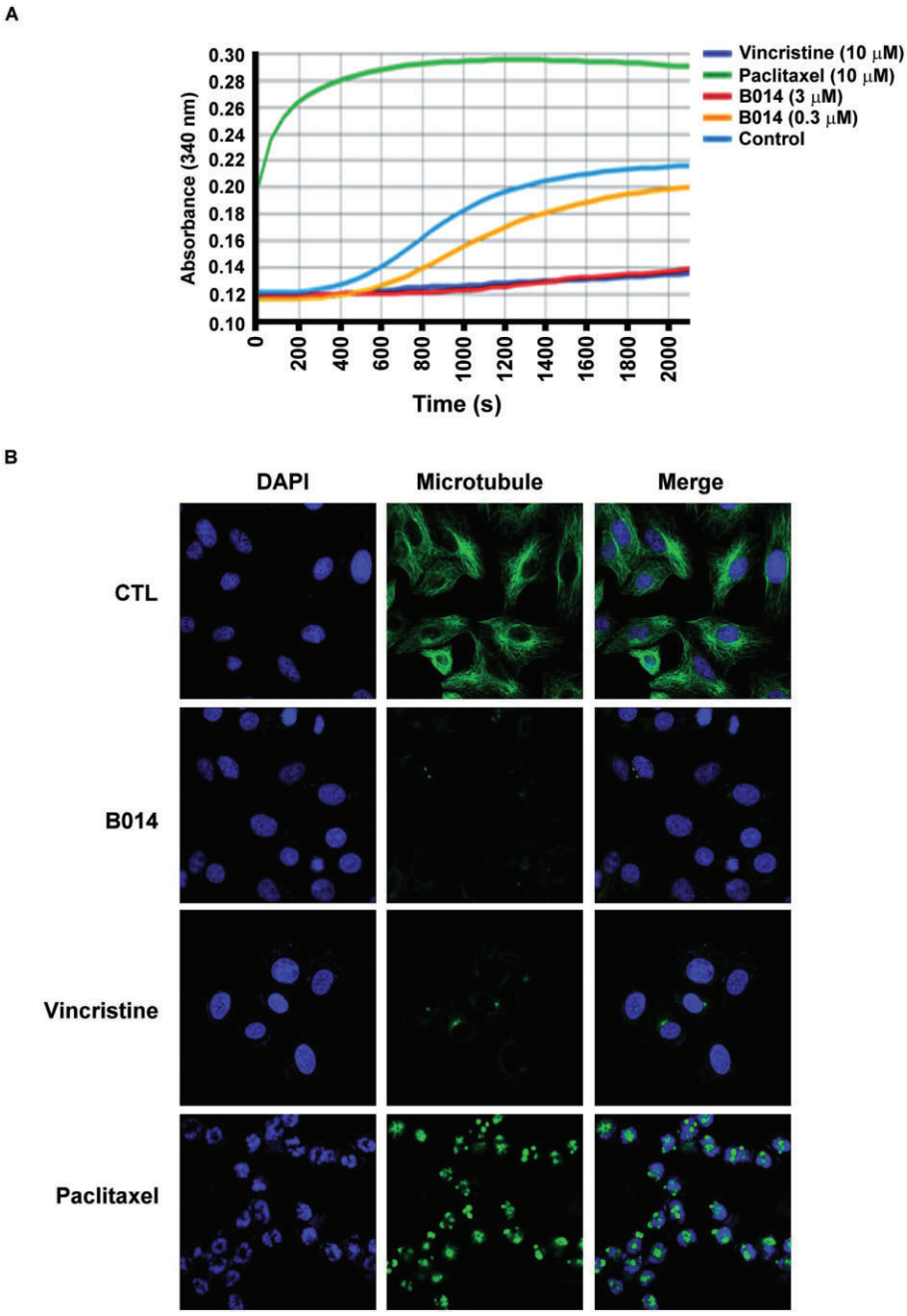

Figure 3

Effect of B014 on microtubule dynamics. (A) Inhibition of tubulin polymerization by *in vitro* tubulin polymerization assay kit. Tubulin proteins (>99% purity) were suspended in reaction buffer in the presence or absence of B014 (3.0 or 0.3 μM), paclitaxel (10 μM) or vincristine (10 μM). Assembly of microtubules was determined by measuring absorbance at 340 nm using a spectrophotometer. (B) *A549* cells were treated with vehicle (DMSO), 0.3 μM B014, paclitaxel or vincristine for 24 h. After treatment, microtubules of cells were stained with β-tubulin antibody and FITC-conjugated anti-mouse IgG. Nuclear DNA was visualized by DAPI staining. Microtubule networks were visualized using confocal microscopy. Left, DAPI; middle, microtubule network; right, merged microtubule network and DAPI.

human NSCLC (Ramalingam and Belani, 2004; Bennouna *et al.*, 2008), the worldwide incidence of human NSCLC and subsequent mortalities are increasing, and these treatments have failed to prolong patient survival substantially. Therefore, novel therapeutic agents that have increased efficacy against human NSCLC are required. Here we demonstrate the potential of B014 against human NSCLC *in vitro* and *in vivo*. The 6-aroylquinoline compound B014 (6-(3′,4′,5′-trimethoxybenzoyl)quinoline, MPT0B014), was identified as an anti-cancer agent based on the following structure-activity information. The 3,4,5-trimethoxybenzene moiety plays an important role for antimitotic activity as, for example, in

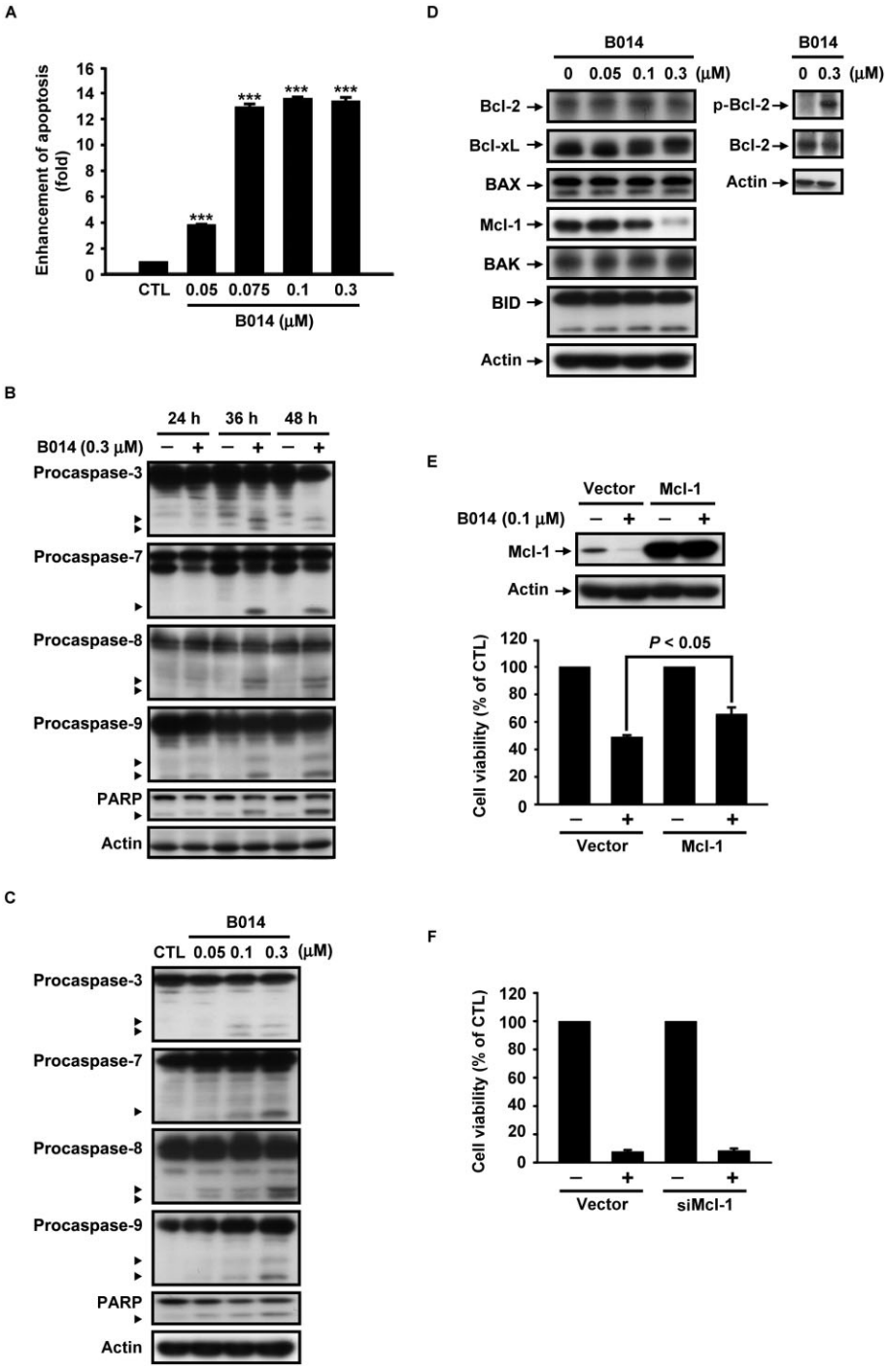

Figure 4

B014 triggers apoptosis in A549 cells. (A) After treatment with various concentrations of B014 for 48 h, the induction of apoptosis was assessed the amounts of oligonucleosomal DNA fragmentation using a Cell Death ELISA^{PLUS} kit. Data shown are means ± SEM. ***$P < 0.001$, compared with the control group. (B) Time-dependent effects of B014 on apoptosis. A549 cells were exposed to 0.3 μM B014 for the indicated times; whole-cell lysates were collected and immunoblotted using indicated antibodies. (C) Concentration-dependent effect of B014 on apoptosis. A549 cells were treated with serial concentrations of B014 for 48 h; whole-cells extracts were prepared and analysed using Western blotting with indicated antibodies. (D) After treatment with various concentrations of B014 for 24 h, A549 cells were harvested, lysed and subjected to SDS-PAGE. Bcl-2, Bcl-xL, BAX, Mcl-1, Bak, BID (left panel), and phosphorylated Bcl-2 (p-Bcl-2) (right panel), were detected by immunoblotting. (E) Exogenous Mcl-1 overexpression rescued cells from apoptosis. A549 cells were transfected with vector or Mcl-1 plasmid for 24 h and incubated with or without B014 for 48 h. Whole-cell lysates were subjected to Western blot analysis and cell viability was measured using the SRB assay. Data shown are means ± SEM. (F) The effect of down-regulation of Mcl-1 by RNA interference on cell viability of B014 in A549 cells. Cell viability was measured using the SRB assay. Data shown are means ± SEM.

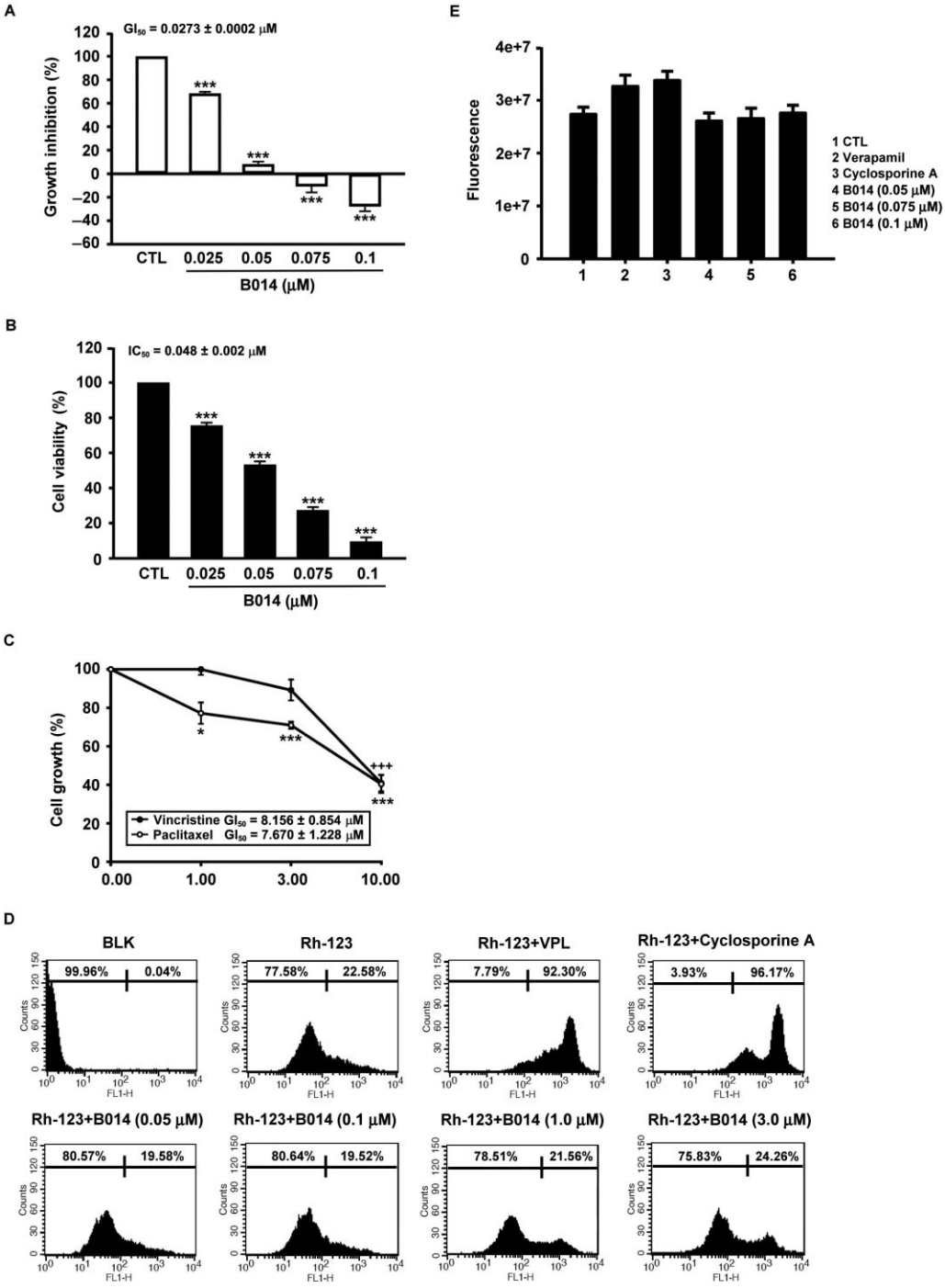

Figure 5

Effect of B014 on P-gp activity. (A) NCI/ADR-RES cells were treated with indicated concentrations of B014 for 48 h, and cell growth was evaluated using the SRB assay. (B) Cytotoxicity was evaluated using the MTT assay. (C) NCI/ADR-RES cells were treated with indicated concentrations of paclitaxel or vincristine for 48 h, and cell growth was determined using the SRB assay. Data shown are means ± SEM of at least three independent experiments. *$P < 0.05$, ***$P < 0.001$, compared with the control group. (D) NCI/ADR-RES cells were treated with or without indicated agents in the presence of 10 μM Rh-123. After incubation for 60 min at 37°C, Rh-123 was detected using flow cytometry. BLK, blank; VPL, verapamil (50 μM); B014, MPT0B014. (E) NCI/ADR-RES cells were treated with or without indicated agents for 30 min and stained with calcein-AM fluorescent dye. Fluorescence was measured by fluorescence microscopy. Data shown are means ± SEM.

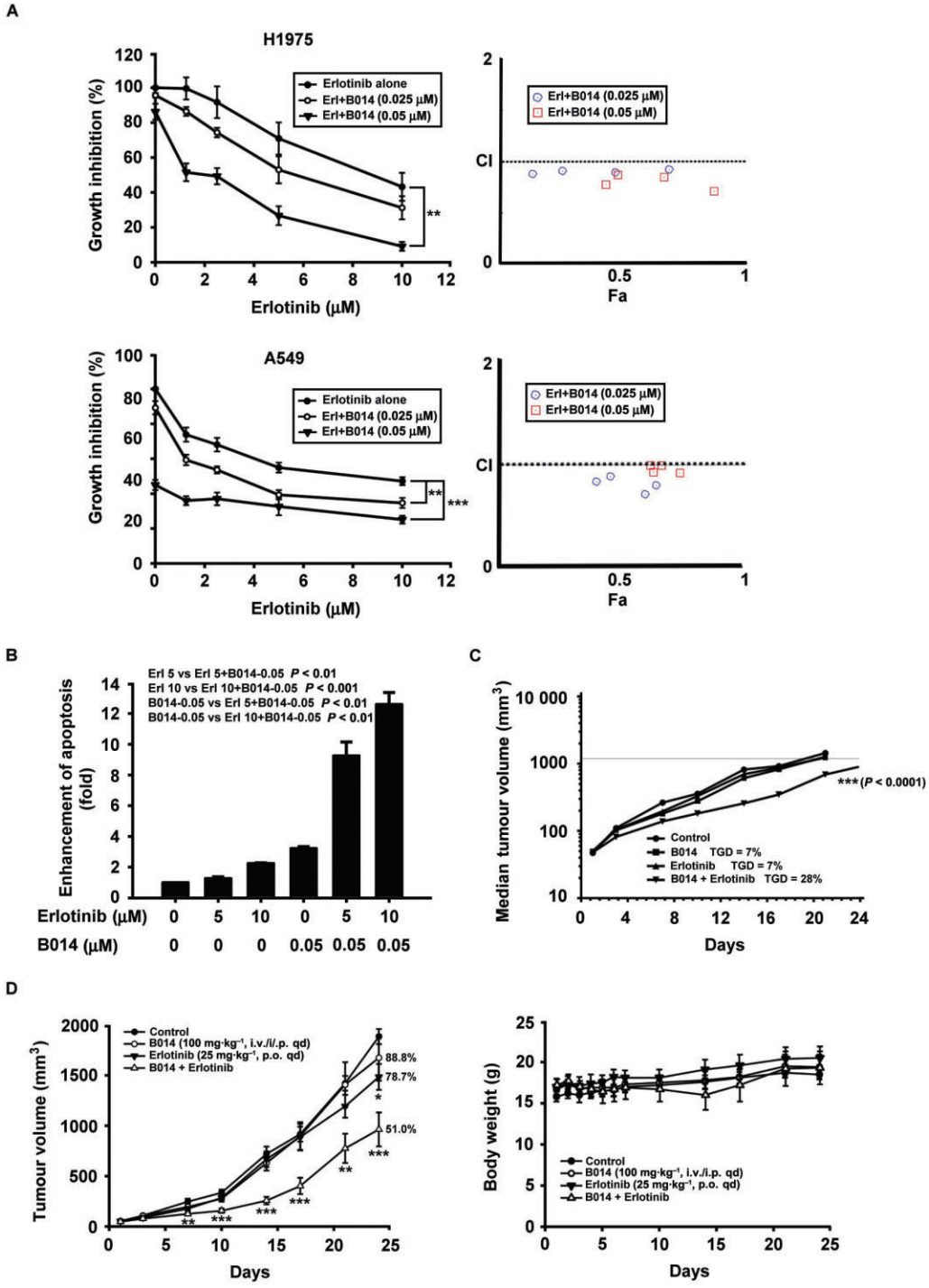

Figure 6

Anti-tumour activity of B014 in combination with erlotinib *in vitro* and *in vivo*. (A) H1975 and A549 cells were incubated with indicated concentrations of B014 or erlotinib alone, or both together for 48 h. Left panel, growth inhibition as determined by SRB assays. Right panel, CI values of the combination therapy of B014 and erlotinib. CI values were calculated using CompuSyn software. Data shown are means ± SEM. $^{**}P < 0.01$, $^{***}P < 0.01$, significantly different as shown. (B) A549 cells were treated with erlotinib (5 and 10 μM) in combination with B014 (0.05 μM) for 48 h, and apoptosis was measured using a Cell Death ELISA^{PLUS} kit. In C and D, *in vivo* assessment of B014 in mice with A5459 xenografts. (C) Percentage of tumour growth delay (TGD) was calculated for treatment groups relative to control group. (D) *Left panel*, tumour growth inhibition curves representing mean ± SE and percentage changes in mean tumour volume (tumour growth inhibition). Data shown are means ± SEM. $^{**}P < 0.01$, $^{***}P < 0.001$, compared with the control group. Right panel, body weights in the experimental groups.

colchicine, combretastatin A-4 and podophyllotoxin. The quinoline ring is a pharmacologically active heterocycle. In order to explore the structure–activity relationships between the quinoline and the trimethoxybenzoyl group, the seven regioisomers of aroylquinoline, 2-, 3-, 4-, 5-, 6-, 7-, 8-aroylquinolines, were prepared and evaluated for anti-proliferative activity. Results indicated the 6-aroylquinoline (B014) showed the highest activity with mean IC_{50} values of 24.4 nM against KB, H460, HT29, MKN45 and KB-vin10 cells and was selected for further investigation on its mode of action. B014 exerted stronger anti-proliferative activity and cytotoxicity against three human NSCLC cell lines than against normal HUVECs, indicating that it exhibits cancer cell-specific cytotoxicity. The IC_{50} values for H1299 cells that lack endogenous p53 or mutant p53 H226 cells were similar to those for A549 cells that have well-characterized p53 expression. Hence, the cytotoxicity of B014 did not depend on the p53 status of NSCLC cells.

It is widely known that microtubule-targeting agents interrupt microtubule dynamics, thereby inducing mitotic arrest and leading to programmed cell death (Jordan and Wilson, 2004). In this study, we focused on the effect of B014 on microtubule dynamics to clarify its anti-cancer mechanism. In general, microtubule-targeting agents directly bind to tubulin and induce stabilization or destabilization of microtubule dynamics (Risinger *et al.*, 2009). As shown in immunofluorescence staining and cell-free polymerization experiments, B014 disrupted the microtubule arrangements in A549 cells and blocked tubulin polymerization, indicating that B014 acts as a microtubule-depolymerizing agent by directly interacting with tubulin.

In our experiments, we found that B014 caused cell cycle arrest in the G2/M phase. Cell cycle progression is tightly regulated by several cyclins, cyclin-dependent kinases and other regulatory mechanisms. Prior to mitosis, cyclin B1 accumulates in the cytoplasm and binds to Cdc2/p34 to form heterodimers to facilitate the inhibitory phosphorylation of Cdc2/p34 at Thr^{14} and Tyr^{15}. However, the critical regulatory step in activating Cdc2/p34 during progression into mitosis appears to be the phosphorylation of Cdc2/p34 at Thr^{161} and dephosphorylation at Thr^{14} and Tyr^{15} (Doree and Galas, 1994; Porter and Donoghue, 2003). Increased phosphorylation of Cdc2/p34 at Thr^{161} and reduced phosphorylation at Tyr^{15} were detected in B014-treated cells. Additionally, the mitosis-specific marker MPM-2 was observed in association with up-regulated cyclin B1. The serine/threonine kinases Aurora kinase A and B are active during mitosis and play a pivotal role in the regulation of centrosomes, chromosome segregation and mitotic spindle assembly (Harrison *et al.*, 2009). Increased expression of Aurora kinase A and B was observed in B014-treated cells. Furthermore, it was reported that cyclin B1 is accumulated from prophase to metaphase and subsequently degraded during anaphase. Additionally, translocation of cyclin B1 to the nucleus at the beginning of mitosis promotes natural cell cycle progression (Porter and Donoghue, 2003). In our study, Western blot analysis showed that B014-induced translocation of cyclin B1 from cytosol to the nucleus, supporting the proposal that B014 induced mitotic arrest in A549 cells.

Most chemotherapeutic agents kill cancer cells by inducing their apoptosis. In the present study, we demonstrated that B014-induced cell death by increasing the number of cytoplasmic histone-associated DNA fragments in a concentration-dependent manner. Current evidence indicates that a variety of apoptotic signals and stimuli are responsible for induction of apoptosis. Most of these pathways result in the activation of caspases, which are synthesized as inactive pro-enzymes, through proteolytic cleavage. Two main apoptotic pathways have been demonstrated, and caspases involved in apoptotic signalling can be categorized as initiator (caspases-8, -9 and -10) or effector caspases (caspases-3, -6 and -7). Caspase-3 is directly involved in cleavage and inactivation of key cellular proteins such as PARP, and is believed to play a key role in apoptosis in many cell types (Fan *et al.*, 2005). In B014-treated A549 cells, PARP cleavage was accompanied by cleavage of pro-caspases-3, -7, -8 and -9, indicating that B014 induces apoptosis by activating a caspase cascade. There are several reports that microtubule-binding agents induced Bcl-2 phosphorylation and caused cell cycle arrest in M phase (Pathan *et al.*, 2001; Sakurikar *et al.*, 2012). We demonstrated that protein level of phosphorylated Bcl-2 was increased by B014 treatment in this study. Mcl-1 is an anti-apoptotic member of the Bcl-2 family of proteins, which are responsible for mitochondrial permeabilization, initiation of caspase cascade and induction of apoptosis (Thomas *et al.*, 2010). Our results showed that B014 decreased Mcl-1 expression in a concentration-dependent manner in A549 cells. Overexpression of exogenous Mcl-1 partially reversed B014-induced cell growth inhibition; in addition, Mcl-1 knockout did not affect B014-induced cell survival. Therefore, we believe that Mcl-1 probably plays an important role in B014-induced apoptosis.

High levels of EGFR have been reported in various epithelial cancers including NSCLC, and its inhibitors have been investigated as first-line or subsequent therapies for advance metastatic NSCLC (Iwai *et al.*, 2012; Stella *et al.*, 2012). The EGFR TK inhibitor (TKI) erlotinib is currently approved for the treatment of metastatic NSCLC and offers a survival benefit (Cataldo *et al.*, 2011). However, resistance to erlotinib eventually occurs. The T790M point mutation in EGFR is most often associated with acquired or secondary resistance to TKIs. The affinity of erlotinib for EGFR is reportedly reduced in H1975 cells carrying this mutation (Moran, 2011). In this study, growth inhibition by erlotinib alone was not notable in A549 and H1975 cells. However, synergism of cytotoxicity between B014 and erlotinib was identified using CompuSyn software (ComboSyn, Inc., Paramus, NJ, USA). Moreover, combined treatment with erlotinib and B014 was effective against A549 cell growth in mice. Median tumour growth and log-rank analysis also demonstrated improved anti-tumour activity of this combination compared with monotherapies, indicating that erlotinib combined with B014 may offer a novel treatment strategy for NSCLC.

This study is the first to demonstrate that B014 possesses anti-proliferative and apoptotic activities against human NSCLC. We demonstrated that B014 caused tubulin depolymerization, mitotic arrest and subsequent apoptosis via a caspase-mediated pathway. Additionally, we observed that B014 was not a P-gp substrate. B014 in combination with the EGFR inhibitor erlotinib showed improved anti-tumour effect against NSCLC *in vitro* and *in vivo*. These findings characterize B014 as a microtubule-destabilizing agent with little

susceptibility to P-gp and thus may offer a novel strategy for treating NSCLC.

Acknowledgements

This work was supported by research grants from the National Science Council of Taiwan NSC 99-2320-B-038-020-MY3 and Taipei Medical University TMU101-AE1-B48.

Conflict of interest

The author, Dr. Jing-Ping Liou, holds the patents for the chemical synthesis of MPT0B014.

References

Akin O, Brennan SB, Dershaw DD, Ginsberg MS, Gollub MJ, Schoder H *et al.* (2012). Advances in oncologic imaging: update on 5 common cancers. CA Cancer J Clin 62: 364–393.

Bareschino MA, Schettino C, Rossi A, Maione P, Sacco PC, Zeppa R *et al.* (2011). Treatment of advanced non small cell lung cancer. J Thorac Dis 3: 122–133.

Bennouna J, Delord JP, Campone M, Nguyen L (2008). Vinflunine: a new microtubule inhibitor agent. Clin Cancer Res 14: 1625–1632.

Bhalla KN (2003). Microtubule-targeted anticancer agents and apoptosis. Oncogene 22: 9075–9086.

Bhat KM, Setaluri V (2007). Microtubule-associated proteins as targets in cancer chemotherapy. Clin Cancer Res 13: 2849–2854.

Breathnach OS, Freidlin B, Conley B, Green MR, Johnson DH, Gandara DR *et al.* (2001). Twenty-two years of phase III trials for patients with advanced non-small-cell lung cancer: sobering results. J Clin Oncol 19: 1734–1742.

Brown ER, Shepherd FA (2005). Erlotinib in the treatment of non-small cell lung cancer. Expert Rev Anticancer Ther 5: 767–775.

Cataldo VD, Gibbons DL, Perez-Soler R, Quintas-Cardama A (2011). Treatment of non-small-cell lung cancer with erlotinib or gefitinib. N Engl J Med 364: 947–955.

Doree M, Galas S (1994). The cyclin-dependent protein kinases and the control of cell division. FASEB J 8: 1114–1121.

Fan TJ, Han LH, Cong RS, Liang J (2005). Caspase family proteases and apoptosis. Acta Biochim Biophys Sin (Shanghai) 37: 719–727.

Francis H, Solomon B (2010). The current status of targeted therapy for non-small cell lung cancer. Intern Med J 40: 611–618.

Harrison MR, Holen KD, Liu G (2009). Beyond taxanes: a review of novel agents that target mitotic tubulin and microtubules, kinases, and kinesins. Clin Adv Hematol Oncol 7: 54–64.

Honore S, Pasquier E, Braguer D (2005). Understanding microtubule dynamics for improved cancer therapy. Cell Mol Life Sci 62: 3039–3056.

Huang HL, Lee HY, Tsai AC, Peng CY, Lai MJ, Wang JC *et al.* (2012). Anticancer activity of MPT0E028, a novel potent histone deacetylase inhibitor, in human colorectal cancer HCT116 cells *in vitro* and *in vivo*. PLoS ONE 7: e43645.

Iwai T, Moriya Y, Shirane M, Fujimoto-Ouchi K, Mori K (2012). Continuous inhibition of epidermal growth factor receptor phosphorylation by erlotinib enhances antitumor activity of chemotherapy in erlotinib-resistant tumor xenografts. Oncol Rep 27: 923–928.

Jordan MA, Wilson L (2004). Microtubules as a target for anticancer drugs. Nat Rev Cancer 4: 253–265.

Kavallaris M (2010). Microtubules and resistance to tubulin-binding agents. Nat Rev Cancer 10: 194–204.

Kilkenny C, Browne W, Cuthill IC, Emerson M, Altman DG (2010). Animal research: Reporting *in vivo* experiments: the ARRIVE guidelines. Br J Pharmacol 160: 1577–1579.

McGrath J, Drummond G, McLachlan E, Kilkenny C, Wainwright C (2010). Guidelines for reporting experiments involving animals: the ARRIVE guidelines. Br J Pharmacol 160: 1573–1576.

Moran C (2011). Importance of molecular features of non-small cell lung cancer for choice of treatment. Am J Pathol 178: 1940–1948.

Munoz-Pinedo C (2012). Signaling pathways that regulate life and cell death: evolution of apoptosis in the context of self-defense. Adv Exp Med Biol 738: 124–143.

Nogales E (2001). Structural insight into microtubule function. Annu Rev Biophys Biomol Struct 30: 397–420.

Pathan N, Aime-Sempe C, Kitada S, Basu A, Haldar S, Reed JC (2001). Microtubule-targeting drugs induce bcl-2 phosphorylation and association with Pin1. Neoplasia 3: 550–559.

Perez EA (2009). Microtubule inhibitors: differentiating tubulin-inhibiting agents based on mechanisms of action, clinical activity, and resistance. Mol Cancer Ther 8: 2086–2095.

Porter LA, Donoghue DJ (2003). Cyclin B1 and CDK1: nuclear localization and upstream regulators. Prog Cell Cycle Res 5: 335–347.

Ramalingam S, Belani CP (2004). Paclitaxel for non-small cell lung cancer. Expert Opin Pharmacother 5: 1771–1780.

Reungwetwattana T, Weroha SJ, Molina JR (2012). Oncogenic pathways, molecularly targeted therapies, and highlighted clinical trials in non-small-cell lung cancer (NSCLC). Clin Lung Cancer 13: 252–266.

Risinger AL, Giles FJ, Mooberry SL (2009). Microtubule dynamics as a target in oncology. Cancer Treat Rev 35: 255–261.

Sakurikar N, Eichhorn JM, Chambers TC (2012). Cyclin-dependent kinase-1 (Cdk1)/cyclin B1 dictates cell fate after mitotic arrest via phosphoregulation of antiapoptotic Bcl-2 proteins. J Biol Chem 287: 39193–39204.

Sangodkar J, Katz S, Melville H, Narla G (2010). Lung adenocarcinoma: lessons in translation from bench to bedside. Mt Sinai J Med 77: 597–605.

Siegel R, Naishadham D, Jemal A (2012). Cancer statistics for Hispanics/Latinos, 2012. CA Cancer J Clin 62: 283–298.

Stella GM, Luisetti M, Inghilleri S, Cemmi F, Scabini R, Zorzetto M *et al.* (2012). Targeting EGFR in non-small-cell lung cancer: lessons, experiences, strategies. Respir Med 106: 173–183.

Taylor RC, Cullen SP, Martin SJ (2008). Apoptosis: controlled demolition at the cellular level. Nat Rev Mol Cell Biol 9: 231–241.

Thomas LW, Lam C, Edwards SW (2010). Mcl-1; the molecular regulation of protein function. FEBS Lett 584: 2981–2989.